Fuel 398 (2025) 135500

Contents lists available at ScienceDirect

Fuel

journal homepage: www.elsevier.com/locate/fuel

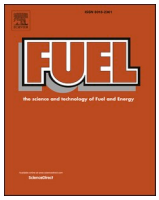

Full Length Article

Detailed analysis of coke precursor formation in catalytic perhydro benzyltoluene dehydrogenation processes

Julian Henseler [a], Timo Schärfe [a], Julien Steffen [b], Andreas Görling [b,c], Michael Geißelbrecht [a], Peter Wasserscheid [a,d,e,*]

[a] Forschungszentrum Jülich GmbH, Helmholtz-Institute Erlangen-Nürnberg for Renewable Energy, (IET-2), Cauerstraße 1, 91058 Erlangen, Germany
[b] Lehrstuhl Für Theoretische Chemie, Friedrich-Alexander-Universität Erlangen-Nürnberg, Egerlandstraße 3, 91058 Erlangen, Germany
[c] Erlangen National High Performance Computing Center (NHR@FAU), Martensstr. 1, D-91058 Erlangen, Germany
[d] Lehrstuhl Für Chemische Reaktionstechnik, Friedrich-Alexander-Universität Erlangen-Nürnberg, Egerlandstraße 3, 91058 Erlangen, Germany
[e] Forschungszentrum Jülich GmbH, Institut Für Nachhaltige Wasserstoffwirtschaft, Am Brainergy Park 4, 52428 Jülich, Germany

ARTICLE INFO

Keywords:
Hydrogen
LOHC
Benzyltoluene
Chromatography
High resolution mass spectrometry
petroleomics

ABSTRACT

Fuel-like handling, good hydrogen storage capacity and low-pressure operations for charging (at <8 bar) and discharging (at <5 bar) make Liquid Organic Hydrogen Carrier (LOHC) systems an interesting option for hydrogen storage and transport in a future hydrogen economy. One important aspect of all LOHC technologies is the long-term use of the carrier material in many repetitive storage cycles. This requires a minimization of side product formation in all process steps involved. Heavy-boiling side products are in addition problematic as they may remain on the catalyst in gas phase dehydrogenation reactions, where they are converted into coke, which blocks the active sites of the catalyst. In contrast, in liquid phase LOHC dehydrogenation processes, high boiling side products are washed off the catalyst surface and are found dissolved in the LOHC mixture. This enables their analytical identification and quantification. A more detailed understanding of the coke precursor formation enables the development of LOHC purification processes and can give access to a knowledge-based optimization of the applied catalyst materials or process conditions. In this study we present a multi-instrumental analytic approach (GC-FID, HPLC-DAD, HRMS, NMR) to study in detail high-boiler formation in the liquid phase dehydrogenation of perhydro benzyltoluene (H12-BT) under purposely applied very harsh conditions. Our work reveals the structure of so far unidentified side products and gives new insight into the mechanism of high-boiler formation on a commercial Pt on alumina dehydrogenation catalyst.

1. Introduction

The role of hydrogen in reshaping our current energy infrastructure towards less greenhouse gas emissions is undisputed. According to the hydrogen roadmap of the European Union, for example, “the energy transition in the EU will require hydrogen at large scale” [1]. However, the large-scale handling of elemental hydrogen, especially the large-scale storage and transport, comes with significant technical challenges. Elemental hydrogen storage requires high pressures or cryogenic cooling to achieve technically viable volumetric energy densities [2–5]. Therefore, the commercial rollout of alternative hydrogen logistic solutions based on hydrogen derivatives, such as the liquid organic hydrogen carrier (LOHC) technology, is gaining more and more attention [6]. The LOHC technology enables high volumetric hydrogen densities at ambient conditions without the need for pressurization or liquefaction thus enabling a further use of the existing fuel infrastructure (tank farms, tank ships, etc.) for the future hydrogen economy.[7,8] The underlying storage principle builds on the reversible catalytic hydrogenation/dehydrogenation of hydrogen-lean/hydrogen-rich organic carrier molecules. In the exothermal hydrogenation processes, hydrogen reacts with the hydrogen lean LOHC molecule converting it into its corresponding hydrogen-rich counterpart. Both the hydrogen-rich and the hydrogen-lean molecules are liquids at ambient conditions. At times and locations of hydrogen or energy demand, the hydrogen-rich molecule can release the bound hydrogen in a catalytic endothermal dehydrogenation reaction. This unloading step produces hydrogen and the initial hydrogen-lean molecule, thus closing the LOHC storage cycle. In this study we investigate the LOHC system benzyltoluene (H0-BT)/perhydro benzyltoluene (H12-BT). The H0–BT/H12-BT system is especially interesting due to its high hydrogen storage capacity, good

* Corresponding author.

https://doi.org/10.1016/j.fuel.2025.135500
Received 31 January 2025; Received in revised form 7 April 2025; Accepted 24 April 2025
Available online 30 April 2025

commercial availability (H0-BT is used as heat transfer fluid since the 1960s), wide liquid range and favorable safety profile (e.g. low flammability) [9–12].

The catalytic dehydrogenation reaction that releases hydrogen from LOHC systems is typically promoted by a heterogeneous precious metal on support catalyst. Depending on the type of LOHC carrier and depending on the pressure and temperature conditions of the dehydrogenation, this reaction can take place with the LOHC carrier being fully evaporated, partly evaporated or mostly in the liquid phase. This difference also decides the nature and fate of high-boiling side products formed in the process. In this context high-boiling side products refers to substances with a substantially higher boiling point than the main compound. In the case of the methylcyclohexane (MCH)/toluene (TOL) LOHC system, all LOHC compounds are gaseous during the dehydrogenation process and as investigated by Alhumaidan et al. high-boiling side products accumulate at the catalyst surface in form of carbonaceous deposits, also known as coke [13,14]. Such deposits do not only lead to a certain (typically very small) loss of the LOHC carrier material. More relevant, they deactivate the dehydrogenation catalyst which typically contains Pt or Pd nanoparticles as the active component supported on aluminum oxide [13,15,16]. As these precious metal catalysts represent a part of the capital investment for the hydrogen release system, catalyst deactivation by strongly adsorbing and high-boiling side products should be avoided [17,18]. These critical side-products form in rearrangement, condensation or deep dehydrogenation reactions and are typically characterized by an increased molecular weight and aromaticity [17]. We define deep dehydrogenation in the context of the LOHC technology as a dehydrogenation process that leads to undesired (i.e., high-boiling or high-melting) side-products by additional hydrogen abstraction from the intended hydrogen-lean compound of the respective LOHC system.

In contrast, Guisnet et al. found out that for liquid phase dehydrogenation reactions, such as the hydrogen release from H12-BT, the formation of carbonaceous deposits on the catalyst is not dependent on the side-product's boiling point, but on its solubility in the hot reaction mixture [17]. Since the aromaticity of these side-products is high their solubility in the aromatic H0-BT reaction product is also high. Therefore these high-boiling coke precursors are washed off the catalyst surface and dissolve in the liquid reaction mixture [19]. Highly remarkably, this phenomenon leads to very long catalyst lifetimes in liquid phase LOHC dehydrogenation processes. Note that the washed-off, condensed side-products have not yet formed carbonaceous deposits but represent relevant intermediates towards their formation. Thus, a deep analysis of these molecules can help us to understand mechanistic pathways towards coke formation in general. With ongoing deep dehydrogenation and condensation, the solubility of coke precursors in hot aromatic solvents reduces [20] and their adsorption on the catalyst becomes much more likely also in liquid phase processes [21–23]. This is why periodic purification of the LOHC system from high-boilers (e.g. by adsorption or by distillation steps) helps to keep the catalyst activity high in processing recycled LOHC systems. In addition, higher shares of dissolved heavy side products in the LOHC system may alter the otherwise favorable physicochemical conditions of the LOHC system, i.e. by increasing melting point or dynamic viscosity [24,25].

In the following, we will focus our considerations on the above-described, industrially highly relevant H0-BT/H12-BT based LOHC system. For this system, Rüde et al. have recently described that the formation of methylfluorene isomers (MeFl) by deep dehydrogenation of H0-BT represents the first and most relevant step in the high-boiling side products formation [12]. The MeFl concentration was found by these authors to subsequently increase in the LOHC mixture during multiple dehydrogenation/hydrogenation cycles with the same LOHC material. As MeFl formation requires H0-BT as the starting material, we conclude that most high-boiling side-products are formed during the dehydrogenation process where over prolonged times H0-BT-rich reaction mixtures are present at high temperature and low hydrogen partial pressure conditions. First studies have been conducted to improve dehydrogenation catalyst systems to reduce the MeFl formation [26]. This research direction holds great promise for a future reduction or even elimination of high-boiling side product formation.

From an application side, the German Institute for Standardization has published an LOHC specification (DIN SPEC) that regulates the maximum content of MeFl and heavier hydrocarbons to 5–10 wt%.[27] Although MeFl is a viable LOHC compound itself[28], technical LOHC mixtures should be inspected for condensation and deep dehydrogenation products in the context of quality control to keep melting points and viscosities within the specified limits. Apart from this, it remains highly desirable to understand the whole spectrum of hydrocarbons within a given technical LOHC sample as MeFl compounds are expected to act as starting points for further condensation reactions. A detailed knowledge on structures and quantities of heavy side products will help to optimize catalyst and process conditions in the dehydrogenation processes and will allow us to develop targeted processes for heavies' removal in periodic LOHC cleaning to stay within the specified purity limits over wide operation periods and over multiple cycles.

Until now, gas chromatography coupled to a flame ionization detector (GC-FID) is the state-of-the-art method for main component and side product analysis in the H0–BT/H12–BT LOHC system [27]. Its main advantage is its universal and sensitive detection of hydrocarbons, allowing for an easy quantification workflow. However, GC-FID is said to be limited to volatile molecules with a mass of less than 300 Da [29–31]. This limitation to lighter, more volatile molecules in GC has led to the preferred use of alternative analytical methods in fields that are dealing with the analysis of less volatile hydrocarbons. Therefore, liquid chromatography (LC) coupled to ultraviolet absorption (UV) or fluorescent (FLD) detection is widely used in polycyclic aromatic hydrocarbon (PAH) analysis [30,32,33]. In analytical petrochemical research, oil samples consisting of a vast number of different hydrocarbons are investigated over a very wide boiling range. Therefore, to overcome the limitations of GC, either direct infusion high resolution mass spectrometry (DI-HRMS) or LC-HRMS are the method of choice [34,35].

The same methods will be applied in this work to reveal the nature and quantity of heavy-boiling side products from thermally stressed samples of the H0-BT/H12-BT LOHC system. Additionally, simulations of UV–Vis spectra using density-functional theory are used to confirm proposed molecular structures. With our multi-instrumental approach, we identify and quantify previously unknown side products in the H0-BT/H12-BT system, i.e. substances with a mass of more than 350 Da. This gives invaluable information to design better catalysts, optimize reaction conditions, and develop purification processes for a further optimization of hydrogen release from H12-BT and structurally related LOHC systems.

2. Methods

2.1. HPLC-DAD/HPLC-DAD-MS

In this study, an Agilent 1260 Infinity II LC system was used, which was connected in series to an Agilent 1260 DAD HS detector and a Bruker compact quadrupole – time of flight mass spectrometer (Q-TOF MS). The Q-TOF MS was equipped with a Bruker Apollo II atmospheric pressure photoionization (APPI) source. A dopant (chlorobenzene) was added at 20 μL min^{-1} to the LC flow prior to APPI.

Analytical scale measurements were performed using an Agilent Zorbax Original C18 column (100x4.6 mm; 5 μm). 1 μL of undiluted LOHC sample was injected. The mobile phase consisted of 97 % acetonitrile (ACN) and 3 % dichloromethane (DCM) in the first 4 min. Until 12 min the DCM content of the mobile phase was increased to 28 %. Until 22 min the DCM content was increased to 100 %. The solvent composition was held at 100 % DCM until 26 min and then immediately reduced to 97 % ACN until 30 min. The flow of the mobile phase was set to 0.6 mL min^{-1}.

Semi-preparative sample separation was performed on an Agilent Zorbax Original C18 column (250x9.4 mm; 5 μm). 30 μL of undiluted LOHC sample was injected. The gradient of the mobile phase was similar to the one used in the analytical measurements. Except, the second increase of DCM to 100 % was performed within 12 to 13 min after injection. The DCM content of the mobile phase was held at 100 % until 16 min and immediately returned to 97 % ACN and held until 19 min. The flow of the mobile phase was set to 5 mL min^{-1}. For the semi-preparative fraction collection an Agilent 1260 FC-AS fraction collector was used.

2.2. Direct infusion MS

For direct infusion MS, 10 μL of sample were diluted in 5 mL DCM and injected at 0.05 mL min^{-1} into the MS using a syringe pump. Chlorobenzene was added at 20 μL min^{-1} prior to APPI.

2.3. HT-GC-FID/HT-GC–MS

For high temperature-GC-FID (HT-GC-FID) measurements a Bruker-456 GC equipped with a split/splitless injector and a flame ionization detector was used. For sample separation a Restek Rxi 5-HT column (30 m × 0.25 mm × 0.1 μm) was applied. The injector temperature was set to 350 °C, the FID temperature was set to 380 °C. The oven program started at 50 °C with an increase of 15 °C min^{-1} until the final temperature of 380 °C was reached. The final temperature was held for 2 min. 20 μL of sample was diluted in 980 μL DCM. 1 μL of this dilution was then injected into the GC. Hydrogen was used as a carrier gas at a constant flow of 1.7 mL min^{-1}.

For HT-GC–MS measurements a Perkin Elmer Clarus 690 GC was coupled to a Perkin Elmer SQ8T single quadrupole MS. The Clarus 690 GC was equipped with a programmable split/splitless injector (PSSI). The set temperatures, chromatographic column and oven program were the same as for the HT-GC-FID measurements except that Helium was used as a carrier gas at 1 mL min^{-1}.

For measurements following the DIN SPEC 91437[27] method the protocol of the DIN SPEC was adapted by minor modifications. Hydrogen was used as a carrier gas instead of helium and the constant pressure was therefore adjusted to 24.88 psi instead of 22.17 psi. The final temperature was held for 16 instead of 5 min to ensure complete elution of compounds. Therefore, the final length of the method was 25.33 instead of 14.33 min.

In the case of the purposedly stressed p-H0-BT sample dimerization products were the only high-boiling side products identified by GC–MS. The dimerization products were found to elute after the isomeric mixture of dibenzyltoluene (DIN SPEC >14.3 min; updated method >13.6 min). Peaks of dibenzyltoluene isomers and dimerization products were identified using GC–MS and dibenzyltoluene reference material. As the separate evaluation of individual dimerization products was not practical, they were summarized in a quantitative sum parameter. In the case of the DIN SPEC method these dimerization products were quantified by integration and calculation of the relative peak area in comparison to the total peak area of all sample components. In our updated method we used benzo[a]pyrene as a calibration standard for all substances eluting in a retention time window of 14.0 to 16.1 min and coronene for all peaks eluting from 16.1 min until the end of the chromatogram. Benzo[a]pyrene and coronene were chosen due to their high boiling points, similar aromatic structure and similar retention time as the dimerization products (physical properties see Table 1).

Table 1
Boiling point and retention time of the external calibration standards benzo[a]pyrene and coronene.

	Boiling point in °C	Retention time in min (updated method)
Benzo[a]pyrene	496[36]	14.5
Coronene	525[37]	17.6

2.4. UV–VIS spectra simulation

UV–Vis spectra were calculated with the Orca quantum chemistry package, version 6.0.0.[38] The B3LYP functional[39–41] with a def2-SVP basis set [42,43] was used. The DFT-D4 correction was applied for the consideration of dispersion effects [44–46]. The UV–Vis absorption spectra were calculated by the Adiabatic Hessian (AH) method, with the inclusion of intensities arising from vibronic coupling, using the path integral approach[47]. For this, the Hessian matrices of the ground state and the first excited state determined by time-dependent DFT[48] needed to be calculated first and provided a starting point for the spectrum calculation. For the calculations of the spectra, nine additional excited states were included, respectively, and their important vibrational contributions considered, since especially for the larger molecules with extended aromatic systems, also higher excited states lead to absorptions in the relevant energy range. All intermediates were calculated in heptane, modeled by the conductor-like polarizable continuum (C-PCM) solvation model [49]. Within C-PCM, a dielectric constant of 1.923 and a refraction index of 1.387 were used.

2.5. Chemicals

Acetonitrile (LC-MS grade) was acquired from Honeywell. Benzo[a]pyrene (>96 %), coronene (97 %) and chlorobenzene (99.9 %) were purchased from Merck. Dichloromethane (99.9 %) was purchased from Carl Roth. Benzyltoluene and dibenzyltoluene in technical grade were purchased from Eastman Chemical. The platinum on aluminum oxide (metal loading = 0.3 wt%) catalyst (Elemax D102) was purchased from Clariant Produkte GmbH, Bruckmühl, Germany. Table S1 in the ESI gives more information on the catalyst properties.

2.6. LOHC hydrogenation and dehydrogenation sample

For the analysis of side products acting as potential coke precursors, a severely degraded LOHC sample was needed. This sample was produced in a so called 'hot pressure swing reactor' as previously described by Rüde et al [12]. To simplify side product identification pure *para*-H0-BT (p-H0-BT) was used as reactant instead of the technical isomeric mixture of benzyltoluenes that is typically used in commercial hydrogen storage applications. Note, that technical H0-BT consists predominantly of para and ortho isomers with only a small share of meta isomers due to the regioselectivity of the Friedel-Crafts step in its synthesis from toluene and benzyl chloride [50]. We therefore expect, that information gained from p-H0-BT experiments is also valid for the use of technical H0-BT mixtures. Hydrogenation and dehydrogenation experiments were performed at 320 to 325 °C. The hydrogenation of the BT-based LOHC material was initiated by increasing the hydrogen pressure to 30 bar_{H2}, while the dehydrogenation was initiated by decreasing the hydrogen pressure to 0.9 bar_{H2} (3.9 bara total pressure). Within the first 75 h total reaction time H0–BT was hydrogenated and dehydrogenated 6 times (6 loading/unloading cycles). As we assumed that most of the coke precursors of interest for this study are formed during the dehydrogenation step, an elongated dehydrogenation for another 125 h was performed after these hydrogenation/dehydrogenation cycles. Under these conditions the almost fully aromatic carrier material is stressed in presence of the catalyst at 320 to 325 °C at low hydrogen partial pressures. More information on the course of the hydrogenation and dehydrogenation cycles as well as the catalyst performance can be found in Fig. S1 in the ESI. It is important to note that these conditions are not representative for industrial LOHC material use and were chosen in this study to maximize the formation of side products for their easier identification.

After the elongated dehydrogenation the LOHC sample was analyzed for its content of chemically bound hydrogen and a remaining degree of hydrogenation of 3 % was determined by GC-FID which is equivalent to

the hydrogenation/dehydrogenation equilibrium under the applied reaction conditions.[12].

3. Results and discussion

3.1. Qualitative insights into the sample composition

3.1.1. Direct infusion-high resolution mass spectrometry (DI-HRMS)

The first goal of our multi instrumental approach was to qualitatively understand the compositional range of hydrocarbons within the purposedly stressed LOHC sample by using a direct infusion HRMS approach adapted from petroleomics research [35]. It is important to note that the ionization efficiencies of the atmospheric pressure photo ionization (APPI) used in this study and therefore MS intensity is dependent on the molecular structure of the analyte.[51,52] Tests with cycloaliphatic compounds under our ionization conditions showed no detectable ionization (data not shown). However, as the sample is the result of a stress test under elongated dehydrogenation, the content of cycloaliphatic substances is only 3 wt%. These cycloaliphatic substances are not represented in Fig. 1. Furthermore, molecules with low ionization efficiencies may be underrepresented. Nevertheless, since large substances with high aromaticity show high ionization efficiencies in APPI and ionization efficiencies within substance families are similar, APPI-MS allows to observe trends in product distribution. Moreover, the method focusses exactly on the dehydrogenation side products of interest for this study.

A mass spectrum of the DI-HRMS measurement is shown in Fig. S2. The HRMS data were processed in a way that allows us to give in Fig. 1 the double bond equivalents (DBE) in the detected species as a function of their number of carbon atoms. The DBE is a measure for the amount of interconnections between carbon atoms within a given molecule.[35] Consequently, a high DBE at a constant carbon number indicates a high interconnectivity of carbon atoms and therefore a high degree of aromaticity.

Fig. 1 shows that the hydrocarbon composition within the purposedly stressed LOHC sample is shaped around clusters of molecules with a content of 14, 21, 28, 35, and 42 carbon atoms. Among these, especially the C_{14}, the C_{28} and the C_{42} clusters stand out showing the highest MS intensities. All are multiples of 14 which is the carbon content of H0-BT or methylfluorene (MeFl). Therefore, the clusters C_{28} and C_{42} may represent oligomers of H0-BT and/or MeFl formed by intermolecular condensation reactions. The C_{21} and C_{35} clusters are most likely formed through trans alkylation or hydrogenolysis reactions resulting in either the loss or the gain of a benzyl group (C_7). A closer look to the individual clusters shows a distribution of +/- one carbon atom within each cluster. The specific loss or gain of a methyl group was already observed in the toluene/methylcyclohexane (TOL/MCH) LOHC system resulting in benzene or xylene as side products [14]. This type of cracking reaction is a known coke formation pathway mostly catalyzed by acidic sites of the catalyst and has now been shown to be also relevant for the BT-based LOHC system at least under the here applied stress conditions [17].

Within each cluster of molecules with the same number of carbon atoms a distribution of double bond equivalents is observed. This is caused by intramolecular ring closures followed by double bond formation to result in highly condensed side products. Intramolecular condensation of the two adjacent aromatic rings within a benzyltoluene molecule forming MeFl was already observed by Rüde et al [12]. However, our DI-MS data show multiple intramolecular condensation reactions. Therefore, the formation of fluorene-like species is only one of the intramolecular ring closures responsible for the diversity of double bond equivalents shown in Fig. 1. The inter and intramolecular condensation is of specific concern as it generally shifts the carbon composition in the course of the dehydrogenation reaction towards larger and highly condensed molecules.

3.1.2. HPLC diode array detection mass spectrometry (HPLC-DAD-MS)

HPLC-DAD-MS offers the additional advantage of separating sample components and assigning UV–Vis spectral properties to molecular masses. The larger the aromatic system of a molecule, the more their λ_{max} is shifted from the UV towards the visible range. By filtering the HPLC-DAD chromatogram for absorption of light at elevated wavelengths, the molecules of special interest can be differentiated from the aromatic bulk. In combination with the APPI-HRMS detection subsequent to the HPLC-DAD separation, additional structural information on the separated side products is accessible.[53] Therefore, HPLC-DAD-MS is the ideal method to selectively detect the side products of interest in the purposedly stressed LOHC sample.

The HPLC-DAD chromatogram of the stressed LOHC sample filtered

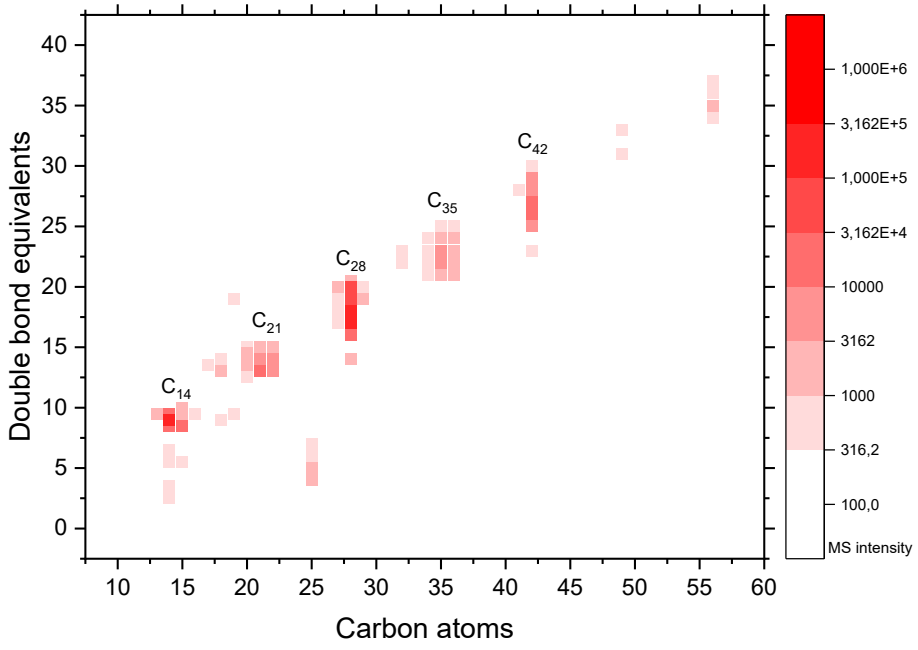

Fig. 1. Double bond equivalents per molecule as a function of their number of carbon atoms obtained by direct injection APPI-HRMS measurements of a purposedly stressed p-H0-BT sample.

for absorption at 254, 350, 500 and 550 nm is shown in Fig. 2. The chromatogram at 254 nm represents the bulk of the sample as the main components like H0-BT and MeFl absorb at this wavelength. The chromatograms filtered for absorbance at 350, 500 and 550 nm reveal groups of side products with a significantly higher degree of inter and intramolecular condensation compared to the initial non-stressed p-H0-BT sample.

Combining this HPLC-DAD information with HRMS and MS/MS information enables a preliminary identification of the side products in our purposedly stressed LOHC sample. The DAD chromatogram filtered for absorption at 254 nm reveals several peaks (see Fig. 2, top line). Peaks 1, 2 and 3 are identified as H0-BT, MeFl and dibenzyltoluene isomers by comparison with commercial reference materials. These substances are visible in the DI-HRMS data of Fig. 1 as main part of the C_{14} and C_{21} clusters. The retention time window of 5 to 7.5 min reveals a mix of substances with a mass of 360 and 358 Da. Due to the lack of resolution within this retention time window the group of substances is labeled as group of peaks 4 (see Fig. 2, top line). The MS/MS spectra of the side products with *m/z* 360 and 358 (see Fig. 3 A and B below) show mass losses of 181 and 179 Da which correspond to the loss of an H0-BT or MeFl fragment. We therefore assume that the products with *m/z* 360 are dimerization products of H0-BT and MeFl. Moreover, we assume that the products with *m/z* 358 are dimerization products of two MeFl molecules.

With a retention time higher than 7.5 min only two more compounds (peak 5 and 6) are present in the 254 nm LC-DAD chromatogram (Fig. 2, top line). These are also the first substances with two intense peaks in the 350 nm chromatogram that also contains three additional peaks (peaks 7, 8 and 9). In the 500 nm chromatogram three additional peaks are present (peaks 10, 11 and 12) of which peaks 11 and 12 show additional absorption properties at 550 nm. Note, that the intensity of peaks 5 to 12 is orders of magnitude smaller compared to peaks 1–4. In fact, peaks 5–12 are only detectable due to their elevated λ_{max}.

Despite their comparatively low signal intensity and therefore likely low concentrations [54], substances 5 to 12 stand out from the bulk of the sample in several ways which make them interesting for a more detailed investigation in the context of a better understanding of coke formation mechanisms. First, these side products have a high degree of intramolecular condensation according to MS information. The side products of peak number 5 and 6 have a mass of 356 Da, peak number 7 a mass of 358 Da and peak numbers 8 to 12 have a mass of 354 Da, meaning these molecules have been formed by one intermolecular and 2 to 4 intramolecular condensation reactions. Secondly, these by–products have a higher λ_{max} of 350 to 550 nm and thirdly they show strong retention on the HPLC column. All these characteristics indicate that these high-boilers represent the largest interconnected aromatic molecules in the stressed LOHC sample under investigation. We consider them therefore most relevant for the LOHC process, as such highly condensed species may harm the activity of the hydrogenation/dehydrogenation catalyst by their irreversible adsorption to the catalyst surface. Therefore, we will focus our further structural studies on these high-boiling compounds.

Note, that the C_{35} and C_{42} substances detected in our DI-MS analysis (Fig. 1) were also detected in the HPLC-DAD-MS measurements. However, we did not perform a detailed structural elucidation for these compounds as they do not exhibit increased λ_{max} or strong retention in the liquid chromatography. While their size might be sufficient for blocking catalyst pores, we assume that these substances are less critical for potential catalyst deactivation in the LOHC process due to their lower degree of intramolecular condensation that results in a much weaker interaction with the catalyst surface.

Fig. 3 A-D depicts the MS/MS spectra of the substances with a *m/z* of 360 to 354. These MS/MS spectra showcase the progressing intramolecular condensation following the initial dimerization reaction. M/z 360 shows multiple intense fragmentation peaks, corresponding to the loss of a CH_3, benzyl, methylbenzyl or H0-BT group (Fig. 3 A). From *m/z* 358 to 354 (Fig. 3 B-D) fragmentation becomes progressively less pronounced. The side reaction responsible for the formation of high-boiling side products could therefore start with an intermolecular connection of two H0-BT or MeFl molecules. This intermolecular connection is then followed by progressive intramolecular condensation towards a mass of 354 Da, the point at which all carbon atoms are interconnected except for a single CH_3 group.

3.2. Detailed structure elucidation of high-boiling side products and their formation pathways

3.2.1. NMR and MS based structure elucidation

HPLC-DAD-MS data show that high-boiler formation starts with dimerization of the initial p-H0-BT and MeFl. However, MS/MS fails to give information on the exact molecular site at which the dimerization reaction takes place. Multiple plausible connections could result in a

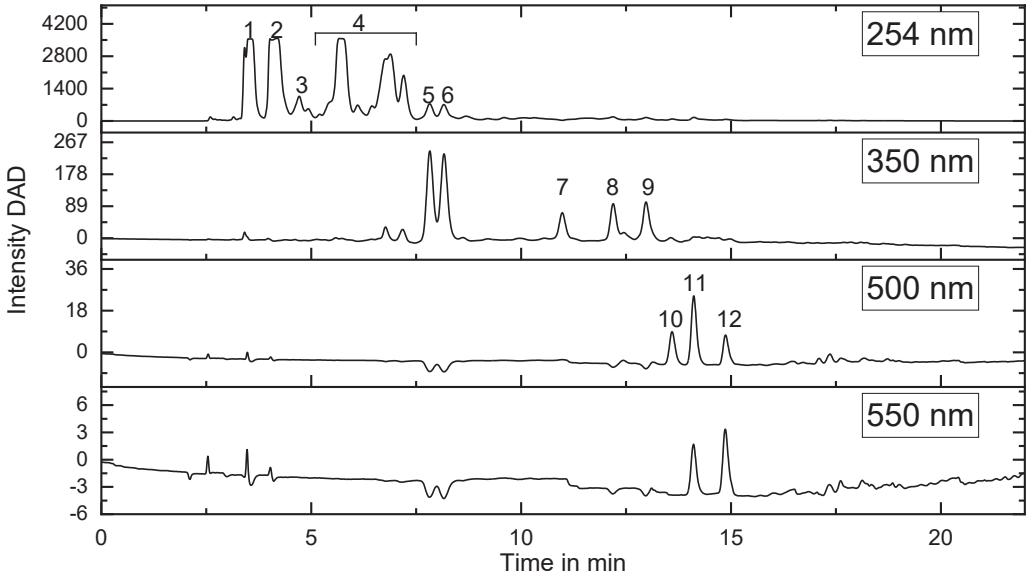

Fig. 2. LC-DAD chromatogram of the purposedly stressed LOHC sample: The DAD chromatograms are filtered for absorption at 254, 350, 500 and 550 nm (from top to bottom). Note that the signal intensity is lower for the higher wavelength measurements.

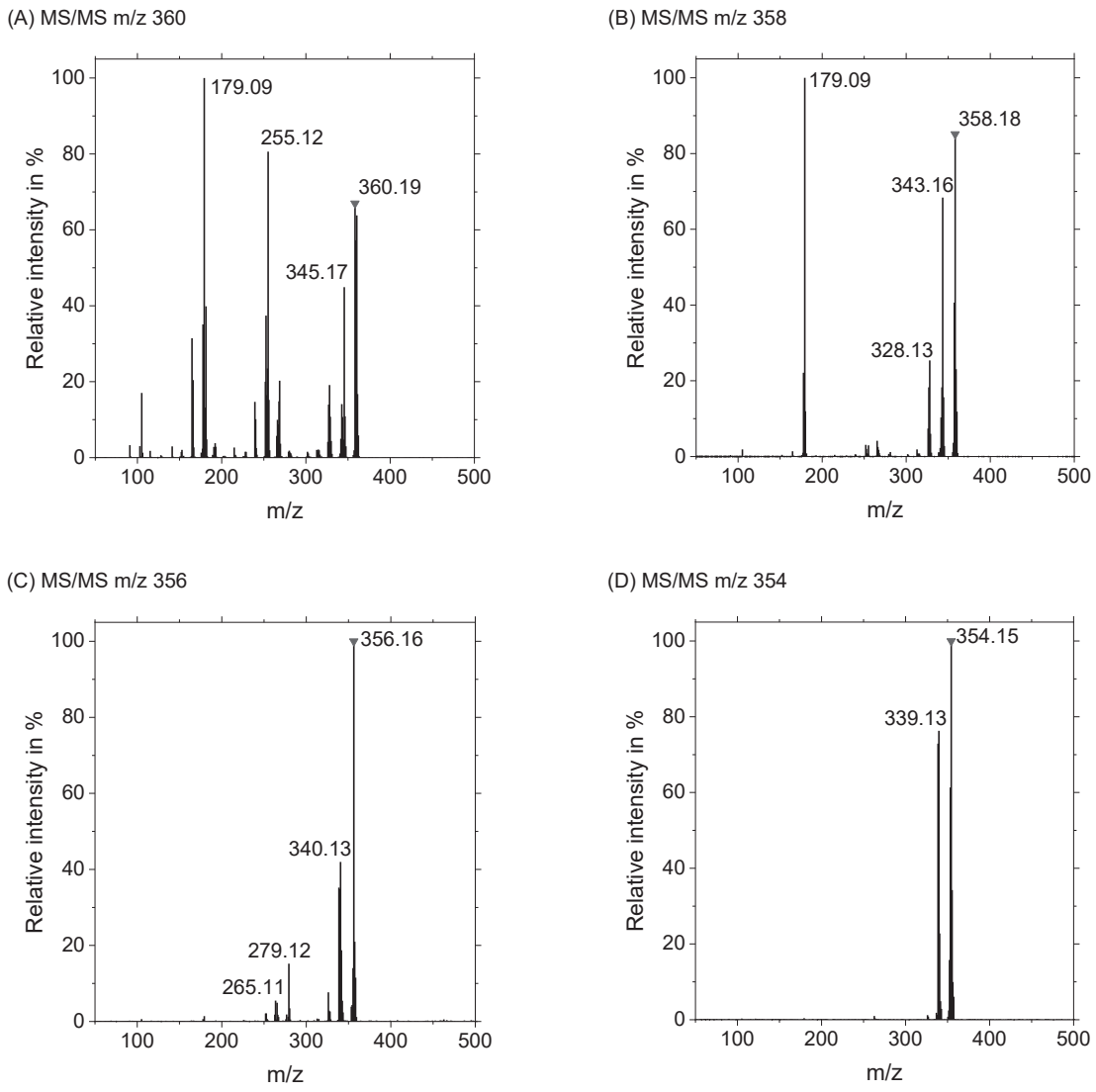

Fig. 3. MS/MS spectra of compounds with *m/z* 354 to 360 found in the purposedly stressed LOHC sample: (A) *m/z* 360; (B) *m/z* 358; (C) *m/z* 356; (D) *m/z* 354.

mass of e.g. 354 Da and in the observed fragmentation pattern shown in Fig. 3 D.

For refining our analysis, we used the insight from previous studies on the reactivity of fluorene derivatives to identify the most plausible reaction mechanisms. This literature states that the C2, C7 and C9 positions are the most reactive sites on a fluorene molecule due to the electron density distribution within the molecule [55–57] However, polymerization of fluorene molecules has been described to require a derivatization of the molecule and the presence of a suitable polymerization catalyst to achieve a specific connection (i.e. a linking of C2 and C7 of two fluorene entities). Other studies report on variable sites for the condensation of fluorene molecules [55] so that one can assume that the H0-BT or MeFl molecules are favorably but not exclusively interconnected via their C2, C7 and C9 carbon atoms during the here-applied extended stress test (i.e. see Fig. 4).

For ease of understanding, we have kept the numbering of the carbon atoms in MeFl, H0–BT, H12-BT and their dimerization products consistent in Fig. 4 and Fig. 5 in the associated text, even if this does not fully correspond to the IUPAC nomenclature. As the MeFl molecule is the main intermediate, H0-BT is viewed as a C11-12 cleaved MeFl molecule in this respect. Changing the atomic numbering in dimerization products would have led to unnecessary confusion for the reader. Therefore, the initial substructures MeFl or H0-BT are color-coded in the following and their respective carbon numbering is used.

The structural investigation of products formed from these dimers (358 Da) by further intramolecular condensation (356 or 354 Da) is particularly interesting as they are characterized by more extensive aromatic systems with higher adsorption abilities to the catalyst surface. Therefore, we decided to isolate substances from peaks 5–12 (Fig. 2) using a semipreparative HPLC method. The ^{1}H- and ^{13}C NMR spectra as well as the UV–Vis spectra of the isolated substances were recorded for a detailed structure elucidation of the isolated substances. In combination with MS/MS information and theoretical calculations, reliable statements can be made about the structure of these high-boiling products in the purposedly stressed LOHC sample and about their formation pathways (see Fig. 5).

The ^{1}H- and ^{13}C NMR spectra of peaks 8 and 9 (354 Da; Fig. S6 and Fig. S7) show exclusively aromatic signals except for a single CH_2 and a single CH_3 group. From this NMR information we deduce that one CH_2 and CH_3 group of the respective MeFl or H0-BT molecules is involved in the dimerization reaction while one CH_2 and CH_3 group remains unaffected. Under this prerequisite, only two pathways for the formation of a final product with a mass of 354 Da are reasonable. The first pathway is based on a C2-C9 connection of two MeFl or H0-BT molecules with an additional connection of the CH_3 group (C14) with an adjacent aromatic molecule (e.g. C8 seen in Fig. 5 D1-4). Intramolecular condensation

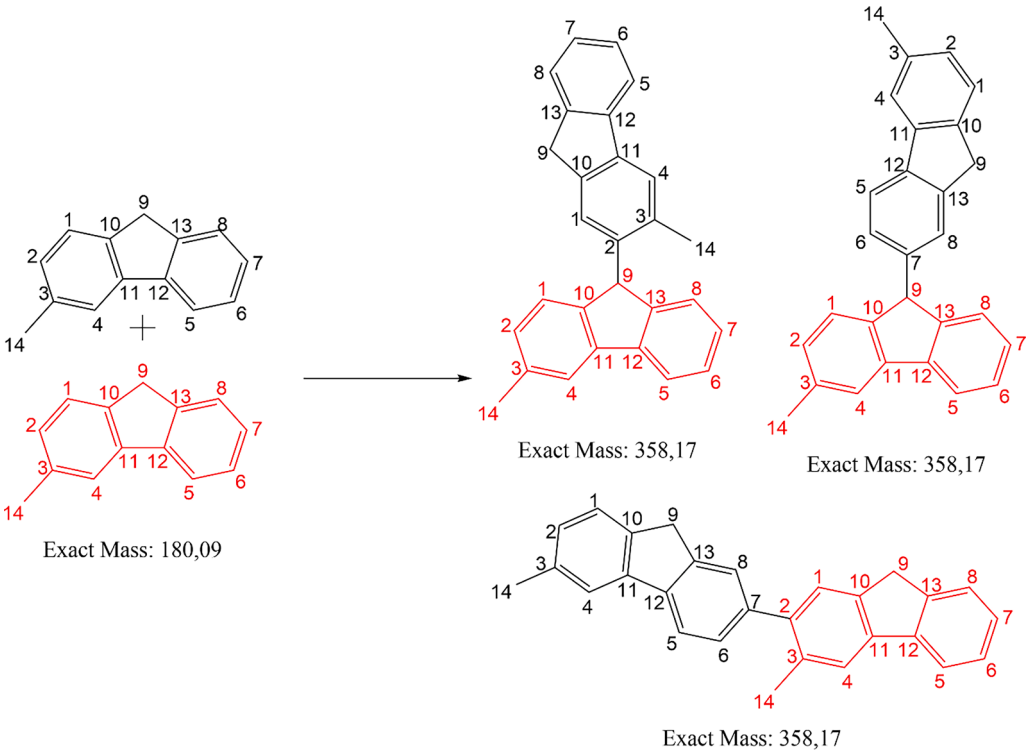

Fig. 4. Examples of dimerization reactions between methylfluorene (MeFl) molecules via their C2, C7 and C9 carbon atoms.

reactions then incorporate the involved CH_2 and CH_3 groups into the aromatic network. The unaffected CH_2 and CH_3 groups are responsible for the remaining aliphatic signals in the NMR spectra. The second pathway is based on the connection of the CH_3 group (C14) with the C9 group and the adjacent aromatic carbon atoms (e.g. C2 and C8 seen in Fig. 5 E1-4).

The NMR spectra recorded from the fractions of peaks 5 and 6 with 356 Da (Fig. S3 and Fig. S4) support these two reaction pathways as they show similar features as the NMR spectra of peaks 8 and 9 (354 Da). Both show exclusively aromatic ^{13}C and ^{1}H signals except for a single CH_2 and a single CH_3 group. This indicates that peaks 5 and 6 are intermediates with a cleaved C11/C12 connection on the pathway towards the formation of the 354 Da products. The H0–BT-like chemical shift of the CH_2 group in the ^{13}C NMR implies a cleaved C11/C12 adjacent to the CH_2 group not involved in the dimerization as seen in Fig. 5 steps D3/E3. The proposed molecular structures of steps D3/E3 are consistent with fragmentation of a methyl, phenyl or benzyl group as the only options, which are exactly the fragmentations observed in Fig. 3C. This further supports the proposed structures.

However, from our NMR and MS data it is not possible to distinguish the reaction pathways D1-4 or E1-4 from the proposed reaction network in Fig. 5. Both pathways result in a 356 or 354 Da molecule consistent with NMR and MS/MS data. Nevertheless, the multitude of 354 and 356 Da isomers detected in the stressed LOHC sample indicates that both reaction schemes may be relevant in the extended dehydrogenation of LOHC material.

The 358 Da substance corresponding to peak 7 demonstrates further options for dimerization reactions in the system. The ^{13}C NMR spectrum shows a total of 14 distinct signals (Fig. S5). However, the HRMS gives a molecular formula of $C_{28}H_{22}$. We conclude that this molecule is a symmetrical dimerization product of MeFl connected via two aromatic carbon atoms (Fig. 5 F2) since the CH_2 and CH_3 signals are both visible in the NMR spectra. This shows that the dimerization of H0-BT or MeFl molecules is feasible at a variety of molecular sites generating a variety of dimerization products with masses of 360 or 358 Da. Most of these regioisomers are part of the unresolved peaks (peak group 4) in the chromatographic separation in Fig. 2. However, within this larger group of molecules, only those connecting C2 with C9 or the methyl group (C14) with C9 result in dimerization products with the potential for further intramolecular condensation forming structures with 356 and 354 Da.

^{1}H- and ^{13}C NMR data of individual group 4 products would give additional information about the linking pattern of the observed dimerization reactions. Unfortunately, the resolution in the HPLC separation was not high enough to allow us to isolate single substances from group 4. Furthermore, ^{1}H- and ^{13}C NMR spectra of peaks 10–12 could not be acquired as the quantities of these substances isolated from the semipreparative HPLC was not high enough for NMR analysis. However, the MS/MS spectra of peaks 8 and 9 are identical to the MS/MS spectra of peaks 10–12 indicating that these are structural isomers.

3.2.2. *Investigation of UV–Vis spectra*

In the following, we aim to validate the proposed structures of Fig. 5 by comparing the experimental UV spectra of the isolated fractions from peak 5–12 with simulated UV spectra of the proposed structures. This comparison has been mainly carried out with regard to their red-shift (λ_{max}) since this indicates the level of intramolecular condensation. The delocalization of electrons in the aromatic systems of different extent leads to a different red-shift of the UV–Vis absorption (>350–550 nm).

Fig. 6 shows on the left side the measured UV–Vis spectra of the substances isolated from peak 9 and 10, both with a mass of 354 Da. Although both molecules are structural isomers, peak 10 comes with an elevated λ_{max} of approx. 500 nm, while peak 9 shows no significant absorption at this wavelength. The right side of Fig. 6 shows a UV–Vis spectrum of the proposed reaction products following the D1-4 or E1-4 routes from Fig. 5, simulated using density-functional theory. Indeed, the structure E4 shows a significantly higher λ_{max} compared to the product D4 in this simulation. We therefore conclude that peaks 8 and 9 with a mass of 354 Da are final products of a C14-C9 dimerization pathway (Fig. 5 E1-4) while peaks 10–12 with elevated λ_{max} are the final products of a C2-C9 dimerization pathway (Fig. 5 D1-4). This finding is

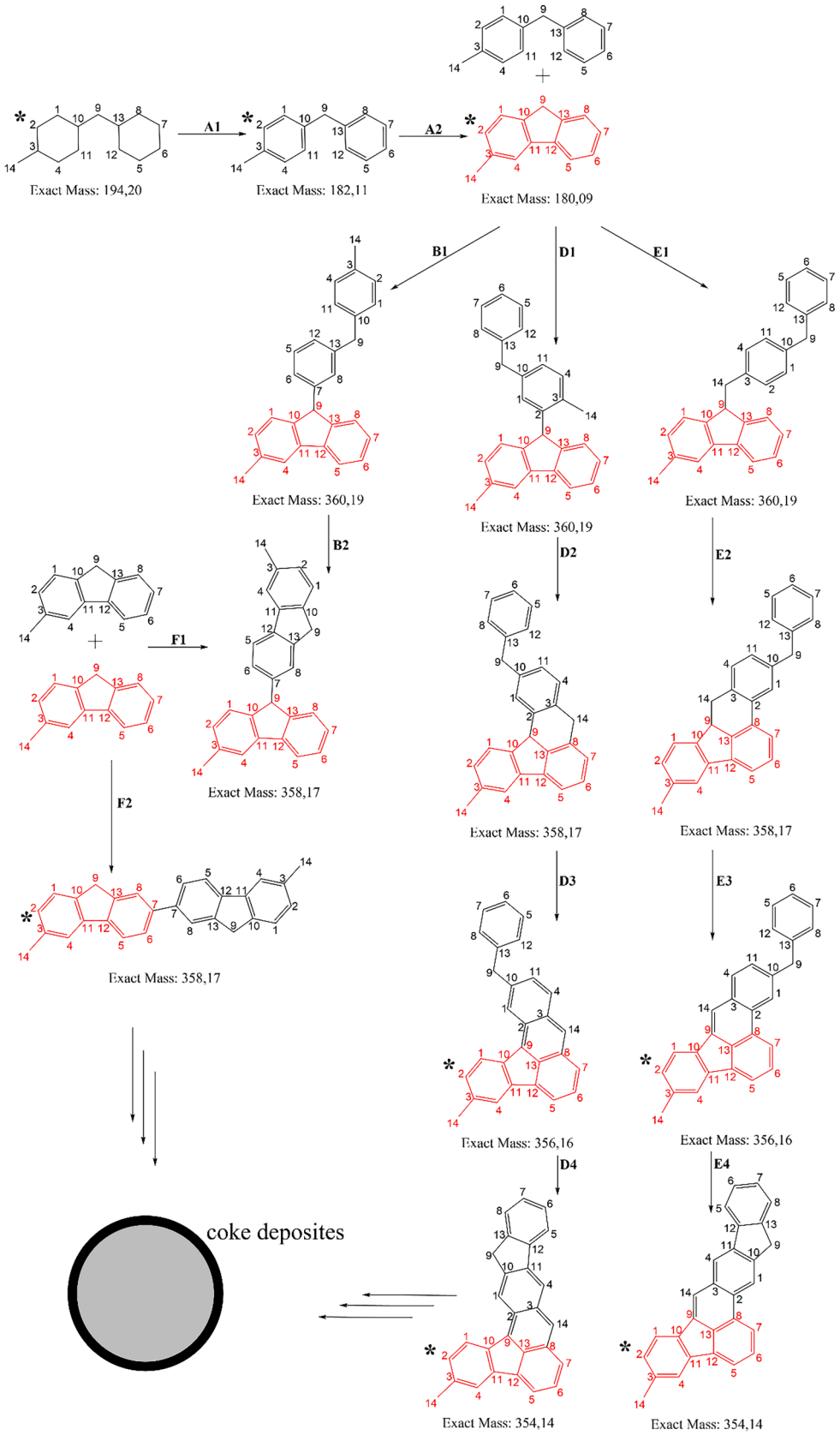

Fig. 5. Proposed reaction network for deep dehydrogenation and coke precursor formation in the H12-BT dehydrogenation under intentional thermal stress. Proposed structures are supported by NMR data or verified with commercial reference material.

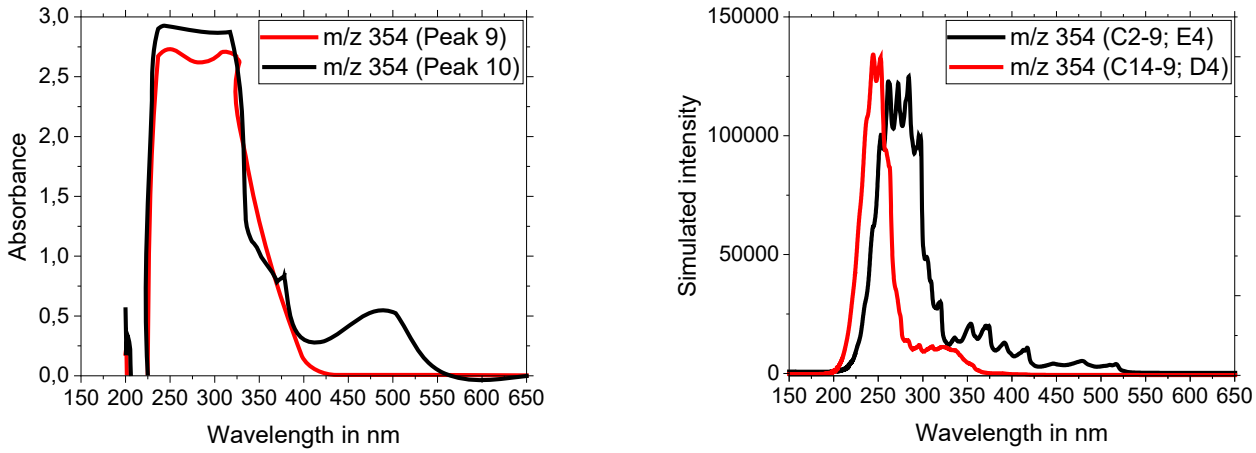

Fig. 6. Experimental UV–Vis spectra of the isolated substances from peak 9 and 10 (in dichloromethane, left) and simulated UV–Vis spectra (in heptane) of the final products with 354 Da following the reaction scheme D1-D4 and E1-E4 (right).

supported by observations from the literature that linear aromatic systems, like the anthracene substructure of E4, show generally higher λ_{max} compared to nonlinear systems like the phenanthrene substructure of D4.[54].

Furthermore, all other UV–Vis spectra of postulated reaction products from the proposed reaction network in Fig. 5 were also simulated using density-functional theory and compared to the experimental UV–Vis in the ESI (Fig. S8–Fig. S11). Substances with a mass of 358 and 360 Da from B1-2, D1–2 and E1-2 were found to have a λ_{max} below 350 nm in both the simulated and experimental UV–Vis spectra. This further supports the proposed structures in Fig. 5.

3.3. *Quantification of dimerization products*

Some of the structures identified in the previous chapters are expected to reduce the catalytic activity of hydrogenation or dehydrogenation catalysts by strong catalyst surface adsorption which leads to at least a temporal blocking of active sites. In order to establish dose–response relationships and to enable description of the expected deactivation effects by quantitative models, reliable quantification of the high-boiling dimerization products is essential. While MS and UV absorption intensity are substance specific and require identical standards for calibration (which are not commercially available), the flame ionization detector (FID) offers a uniform response within the same family of substances. Thereby, GC-FID enables quantification of the identified side-products by using external standards with a similar molecular structure. For sake of simplicity, a sum parameter totaling all dimerization products is determined in this study to avoid the evaluation of individual isomers.

The German Institute for Standardization specification (DIN SPEC) has set a standard procedure for LOHC side product analysis. This method uses GC-FID equipped with a 5 % phenyl stationary phase column.[27] This standard method uses a maximum GC oven temperature of 290 °C and set temperatures of 300 and 325 °C at the injector and detector, respectively. Additionally, a high split ratio is used, and quantification is performed by assuming that the wt.% composition in the sample is equal to the area-% distribution in the chromatogram (correction factor of 1). This method is well suited for main component analysis and for the analysis of side products with similar volatility to the main component H0-BT (i.e. MeFl). It is inaccurate, however, for the quantification of compounds with a substantially higher boiling point than the main compound. Firstly, due to evaporation effects in the injection phase of the analysis, less volatile substances are systematically underestimated.[58] Secondly, the maximum oven temperature of 290 °C inhibits or even prevents the elution of less volatile compounds.

We therefore adjusted our GC-FID setup to reach higher oven temperatures of 380 to 400 °C to be able to fully quantify the previously identified high-boiling dimerization products in the stressed LOHC sample. Additionally, we decreased the split ratio to increase peak heights and used the external reference materials coronene and benzo[a]pyren for quantification purposes.

In the specific case of our thermally stressed LOHC sample the comparison of the established DIN SPEC GC-FID method and our new method optimized for high-boiler determination reveals important differences (see Fig. 7 A and B).

While the analysis according to DIN SPEC determines the overall content of dimerization products to be 4.6 wt%, our optimized method determines it at 7.6 wt%. Additionally, the fraction of strongly condensed dimerization products with a mass of 356 and 354 Da could not be detected using the DIN SPEC method, while the optimized method determined their concentration to be 0.26 wt% in sum (eluting after approximately 18.3–19.6 min). Our optimized GC-FID protocol shows two relevant advantages. Firstly, the separation between dibenzyltoluene peaks and dimerization product peaks is much better than in the DIN SPEC method. Secondly, the peaks of dimerization products are significantly more pronounced. Our results indicate that the high-boiler quantification using the DIN SPEC method can suffer a relevant underestimation of high-boiling aromatic compounds. Thus, we propose our updated method for a more accurate quantification of high-boiling side products in thermally stressed BT-based LOHC samples.

The 7.6 wt% of dimerization products along with 19.8 wt% MeFl quantified in the severely stressed LOHC material greatly surpass the DIN SPEC defined limits for side products in LOHC materials (5–10 wt %). Even though acceptable reaction rates were achieved in the last hydrogenation and dehydrogenation cycle (see ESI Fig. S1) we recommend purification of the LOHC material before further use. The HPLC separation of sample components in Fig. 2 shows that adsorption-based processes seem to be a promising option to separate H0-BT from its side products. Otherwise, more energy intensive purification processes based on distillation need to be used.

4. Conclusion and outlook

In most cases, coke is formed directly on the catalyst surface, which makes the determination of its formation mechanism and the detailed structural analysis of precursor molecules very tedious to impossible. We have shown that in the case of perhydro benzyltoluene dehydrogenation coke precursors are washed off into the liquid aromatic product under the applied hot reaction conditions. This allowed us to study the structure and formation mechanisms of coke precursors by thorough screening of LOHC reaction mixtures.

Using a combination of HPLC-DAD, HRMS and NMR analyses

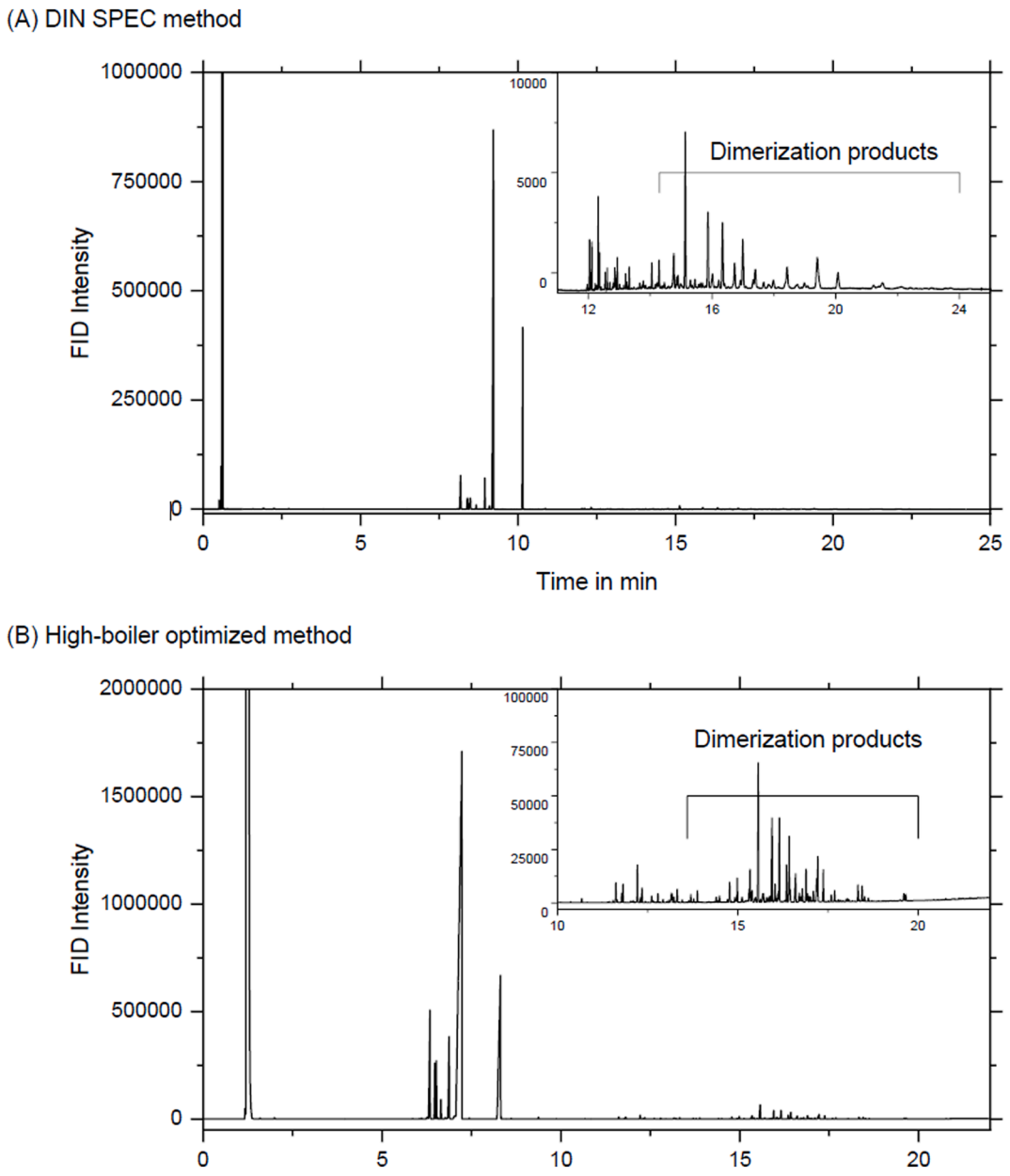

Fig. 7. GC-FID chromatograms of the thermally stressed LOHC sample using the DIN SPEC method (A) and our optimized GC-FID method (B). The retention time window of dimerization products is enlarged in the top right corner of the respective chromatogram. Additional GC-FID chromatograms using our optimized method denominating other sample components and showing a more detailed look onto the dimerization products can be found in the ESI (Fig. S12 and Fig. S13).

together with UV–Vis spectra, simulated using density-functional theory, we demonstrate in this study that the formation of dimerization products is the most prominent side reaction of the Pt-catalyzed H12-BT dehydrogenation reaction besides the formation of MeFl. This side reaction pathway has been found to be highly relevant for coke precursor formation. Herein, MeFl condensates with another MeFl or a H0-BT molecule. This condensation is possible on multiple molecular sites but only the dimerization via the C9 of a MeFl and the C2 or C14 of a MeFl or H0-BT molecule opens a path towards multiple follow-up deep dehydrogenation processes. These processes produce highly condensed aromatic molecules detectable by their increased λ_{max} with an elevated chance to form carbonaceous deposits on the catalyst. Additionally, we improved the current standard method for LOHC material quality control based on GC–FID for a better quantification of dimerization products.

We like to emphasize that the purposedly thermally stressed LOHC sample investigated in this study has been produced in a manner that maximizes high-boiling side product formation to facilitate the development of our analytical methods (multiple hydrogenation/dehydrogenation cycles including a 125 h stress test under very low hydrogen partial pressure at 320 to 325 °C). Furthermore, to avoid complication of the identification process emerging from the technical isomeric mixture of H0-BT, pure *para*-H0-BT was used as reactant in our study. Despite these peculiarities and simplifications our results provide very valuable information on the mechanism of high-boiler and coke formation in the dehydrogenation of BT-based LOHC systems and other related high temperature transformations leading to high-boiling aromatic products. These new insights will inspire the development of better dehydrogenation catalysts, the optimization of dehydrogenation conditions, and the development of LOHC purification technologies, e.g. using selective adsorption technologies.

CRediT authorship contribution statement

Julian Henseler: Writing – review & editing, Writing – original draft, Visualization, Validation, Methodology, Investigation, Formal analysis, Conceptualization. **Timo Schärfe:** Writing – review & editing, Resources, Investigation. **Julien Steffen:** Writing – review & editing, Methodology, Investigation, Formal analysis. **Andreas Görling:** Writing – review & editing, Funding acquisition. **Michael Geißelbrecht:** Writing – review & editing, Supervision, Project administration, Investigation. **Peter Wasserscheid:** Writing – review & editing, Supervision, Resources, Funding acquisition.

Declaration of competing interest

The authors declare the following financial interests/personal relationships which may be considered as potential competing interests: [Julian Henseler reports financial support was provided by Ministry of Economic Affairs, Industry, Climate Action and Energy of the State of North Rhine-Westphalia. Andreas Goerling reports financial support was provided by German Research Foundation. Julien Steffen reports financial support was provided by German Research Foundation. Peter Wasserscheid reports a relationship with Hydrogenious LOHC Technologies GmbH that includes: equity or stocks. If there are other authors, they declare that they have no known competing financial interests or personal relationships that could have appeared to influence the work reported in this paper].

Acknowledgements

The authors acknowledge financial support by the Ministry of Economic Affairs, Industry, Climate Action and Energy of the State of North Rhine-Westphalia through the project “HECTOR”. Additionally, the authors gratefully acknowledge the scientific support and HPC resources provided by the Erlangen National High Performance Computing Center (NHR@FAU) of the Friedrich-Alexander-Universität Erlangen-Nürnberg (FAU) under the NHR project b146dc. NHR funding is provided by federal and Bavarian state authorities. NHR@FAU hardware is partially funded by the German Research Foundation (DFG) - 440719683. The German Research Foundation (DFG) is greatly acknowledged for support through the project number 419654270.

Appendix A. Supplementary data

Supplementary data to this article can be found online at https://doi.org/10.1016/j.fuel.2025.135500.

Data availability

Data will be made available on request.

References

[1] Fuel Cells; Hydrogen 2 Joint Undertaking. *Hydrogen roadmap Europe: a sustainable pathway for the European energy transition*; Publications Office, 2019.
[2] Raab M, Maier S, Dietrich R-U. Comparative techno-economic assessment of a large-scale hydrogen transport via liquid transport media. Int J Hydrogen Energy 2021;46:11956–68.
[3] Reuß M, Grube T, Robinius M, Preuster P, Wasserscheid P, Stolten D. Seasonal storage and alternative carriers: A flexible hydrogen supply chain model. Appl Energy 2017;200:290–302.
[4] Roos TH. The cost of production and storage of renewable hydrogen in South Africa and transport to Japan and EU up to 2050 under different scenarios. Int J Hydrogen Energy 2021;46:35814–30.
[5] Runge, P.; Sölch, C.; Albert, J.; Wasserscheid, P.; Zöttl, G.; Grimm, V. Economic Comparison of Electric Fuels Produced at Excellent Locations for Renewable Energies: A Scenario for 2035. *SSRN Journal* [Online early access]. DOI: 10.2139/ssrn.3623514.
[6] Distel, M. M.; Margutti, J. M.; Obermeier, J.; Nuß, A.; Baumeister, I.; Hritsyshyna, M.; Weiß, A.; Neubert, M. Large-Scale H 2 Storage and Transport with Liquid Organic Hydrogen Carrier Technology: Insights into Current Project Developments and the Future Outlook. *Energy Tech* [Online early access]. DOI: 10.1002/ente.202301042.
[7] Niermann M, Beckendorff A, Kaltschmitt M, Bonhoff K. Liquid Organic Hydrogen Carrier (LOHC) - Assessment based on chemical and economic properties. Int J Hydrogen Energy 2019;44:6631–54.
[8] Rong Y, Chen S, Li C, Chen X, Xie L, Chen J, et al. Techno-economic analysis of hydrogen storage and transportation from hydrogen plant to terminal refueling station. Int J Hydrogen Energy 2024;52:547–58.
[9] Niermann M, Timmerberg S, Drünert S, Kaltschmitt M. Liquid Organic Hydrogen Carriers and alternatives for international transport of renewable hydrogen. Renew Sustain Energy Rev 2021;135:110171.
[10] Kwak Y, Kirk J, Moon S, Ohm T, Lee Y-J, Jang M, et al. Hydrogen production from homocyclic liquid organic hydrogen carriers (LOHCs): Benchmarking studies and energy-economic analyses. Energ Conver Manage 2021;239:114124.
[11] Preuster P, Papp C, Wasserscheid P. Liquid organic hydrogen carriers (LOHCs): Toward a hydrogen-free hydrogen economy. Acc Chem Res 2017;50:74–85.
[12] Rüde T, Dürr S, Preuster P, Wolf M, Wasserscheid P. Benzyltoluene/perhydro benzyltoluene – pushing the performance limits of pure hydrocarbon liquid organic hydrogen carrier (LOHC) systems. Sustainable Energy Fuels 2022;6:1541–53.
[13] Alhumaidan F, Cresswell D, Garforth A. Hydrogen storage in liquid organic hydride: Producing hydrogen catalytically from methylcyclohexane. Energy Fuels 2011;25:4217–34.
[14] Alhumaidan F, Tsakiris D, Cresswell D, Garforth A. Hydrogen storage in liquid organic hydride: Selectivity of MCH dehydrogenation over monometallic and bimetallic Pt catalysts. Int J Hydrogen Energy 2013;38:14010–26.
[15] Clariant International Ltd. Catalysts for Storage of Hydrogen from Renewable Sources via Liquid Organic Hydrogen Carriers (LOHC): EleMax® Series. https://www.clariant.com/de/Solutions/Products/2019/05/21/15/19/EleMax-Series (accessed July 24, 2024).
[16] Kadar J, Gackstatter F, Ortner F, Wagner L, Willer M, Preuster P, et al. Boosting power density of hydrogen release from LOHC systems by an inverted fixed-bed reactor design. Int J Hydrogen Energy 2024;59:1376–87.
[17] Guisnet M. Organic chemistry of coke formation. Appl Catal 2001;212:83–96.
[18] Argyle M, Bartholomew C. Heterogeneous catalyst deactivation and regeneration: A review. Catalysts 2015;5:145–269.
[19] Auer F, Blaumeiser D, Bauer T, Bösmann A, Szesni N, Libuda J, et al. Boosting the activity of hydrogen release from liquid organic hydrogen carrier systems by sulfur-additives to Pt on alumina catalysts. Catal Sci Technol 2019;9:3537–47.
[20] Morantes LR, Percebom AM, Mejía-Ospino E. On the molecular basis of aggregation and stability of Colombian asphaltenes and their subfractions. Fuel 2019;241:542–9.
[21] Ding Z-B, Tommasini M, Maestri M. A topological model for predicting adsorption energies of polycyclic aromatic hydrocarbons on late-transition metal surfaces. React Chem Eng 2019;4:410–7.
[22] Araújo RS, Azevedo D, Cavalcante CL, Jiménez-López A, Rodríguez-Castellón E. Adsorption of polycyclic aromatic hydrocarbons (PAHs) from isooctane solutions by mesoporous molecular sieves: Influence of the surface acidity. Microporous Mesoporous Mater 2008;108:213–22.
[23] Morin C, Simon D, Sautet P. Trends in the chemisorption of aromatic molecules on a Pt(111) Surface: Benzene, naphthalene, and anthracene from first principles calculations. J Phys Chem B 2004;108:12084–91.
[24] Kerscher M, Jander JH, Cui J, Wasserscheid P, Rausch MH, Koller TM, et al. Thermophysical properties of the liquid organic hydrogen carrier system based on diphenylmethane with the byproducts fluorene or perhydrofluorene. Int J Hydrogen Energy 2023;48:29651–62.
[25] Ilyin S, Arinina M, Polyakova M, Bondarenko G, Konstantinov I, Kulichikhin V, et al. Asphaltenes in heavy crude oil: Designation, precipitation, solutions, and effects on viscosity. J Pet Sci Eng 2016;147:211–7.
[26] Bong B, Mebrahtu C, Jurado D, Bösmann A, Wasserscheid P, Palkovits R. Hydrogen loading and release potential of the LOHC system benzyltoluene/perhydro benzyltoluene over S–Pt/TiO 2 catalyst. ACS Eng Au 2024;4:359–67.
[27] DIN. *DIN SPEC 91437:2023-05, Liquid Organic Hydrogen Carrier_(LOHC) auf Basis von Toluol_- Bewertung, Prüfung und Sicherstellung der LOHC-Qualität; Text Englisch*; Beuth Verlag GmbH: Berlin.
[28] Pez, G. P.; Scott, A. R. Hydrogen storage by reversible hydrogenation of pi-conjugated substrates.
[29] Marvin CH, Smith RW, Bryant DW, McCarry BE. Analysis of high-molecular-mass polycyclic aromatic hydrocarbons in environmental samples using liquid chromatography–atmospheric pressure chemical ionization mass spectrometry. J Chromatogr A 1999;863:13–24.
[30] Cai S-S, Syage JA, Hanold KA, Balogh MP. Ultra performance liquid chromatography-atmospheric pressure photoionization-tandem mass spectrometry for high-sensitivity and high-throughput analysis of U.S. Environmental Protection Agency 16 priority pollutants polynuclear aromatic hydrocarbons. Anal Chem 2009;81:2123–8.
[31] Adeniji, A. O.; Okoh, O. O.; Okoh, A. I. Analytical Methods for Polycyclic Aromatic Hydrocarbons and their Global Trend of Distribution in Water and Sediment: A Review. In *Recent Insights in Petroleum Science and Engineering*; Zoveidavianpoor, M., Ed.; InTech, 2018.
[32] Benigni P, DeBord JD, Thompson CJ, Gardinali P, Fernandez-Lima F. Increasing polyaromatic hydrocarbon (PAH) molecular coverage during fossil oil analysis by combining gas chromatography and atmospheric-pressure laser ionization fourier transform ion cyclotron resonance mass spectrometry (FT-ICR MS). Energy Fuels 2016;30:196–203.

[33] Lung S-C-C, Liu C-H. Fast analysis of 29 polycyclic aromatic hydrocarbons (PAHs) and nitro-PAHs with ultra-high performance liquid chromatography-atmospheric pressure photoionization-tandem mass spectrometry. Sci Rep 2015;5:12992.
[34] Heshka NE. Applications of high performance liquid chromatography in the petroleomic analysis of crude oil: A mini-review. Energy Fuels 2021;35:18104–15.
[35] Marshall AG, Rodgers RP. Petroleomics: the next grand challenge for chemical analysis. Acc Chem Res 2004;37:53–9.
[36] International Labour Organization. *BENZO(a)PYRENE: International Chemical Safety Card*, 2021.
[37] Weast RC, Grasselli JG, editors. Handbook of data on organic compounds. 2. ed. Boca Raton: CRC Press; 1992.
[38] Neese F. Software update: The ORCA program system—Version 5.0. WIREs Comput Mol Sci 2022;12.
[39] Stephens PJ, Devlin FJ, Chabalowski CF, Frisch MJ. Ab initio calculation of vibrational absorption and circular dichroism spectra using density functional force fields. J Phys Chem 1994;98:11623–7.
[40] Lee C, Yang W, Parr RG. Development of the Colle-Salvetti correlation-energy formula into a functional of the electron density. Phys Rev B 1988;37:785–9.
[41] Becke AD. Density-functional thermochemistry. III. The role of exact exchange. J Chem Phys 1993;98:5648–52.
[42] Weigend F. Accurate Coulomb-fitting basis sets for H to Rn. Phys Chem Chem Phys 2006;8:1057–65.
[43] Weigend F, Ahlrichs R. Balanced basis sets of split valence, triple zeta valence and quadruple zeta valence quality for H to Rn: Design and assessment of accuracy. Phys Chem Chem Phys 2005;7:3297–305.
[44] Caldeweyher E, Ehlert S, Hansen A, Neugebauer H, Spicher S, Bannwarth C, et al. A generally applicable atomic-charge dependent London dispersion correction. J Chem Phys 2019;150:154122.
[45] Caldeweyher E, Mewes J-M, Ehlert S, Grimme S. Extension and evaluation of the D4 London-dispersion model for periodic systems. PCCP 2020;22:8499–512.
[46] Caldeweyher E, Bannwarth C, Grimme S. Extension of the D3 dispersion coefficient model. J Chem Phys 2017;147.
[47] Souza, B. de; Neese, F.; Izsák, R. On the theoretical prediction of fluorescence rates from first principles using the path integral approach. The Journal of Chemical Physics **2018**, 148, 34104.
[48] Souza de B, Farias G, Neese F, Izsák R. Predicting phosphorescence rates of light organic molecules using time-dependent density functional theory and the path integral approach to dynamics. J Chem Theory Comput 2019;15:1896–904.
[49] Tomasi J, Mennucci B, Cammi R. Quantum mechanical continuum solvation models. Chem Rev 2005;105:2999–3093.
[50] Kim TW, Jo Y, Jeong K, Yook H, Han JW, Jang JH, et al. Tuning the isomer composition is a key to overcome the performance limits of commercial benzyltoluene as liquid organic hydrogen carrier. J Storage Mater 2023;60:106676.
[51] Robb; Covey; Bruins. Atmospheric pressure photoionization: an ionization method for liquid chromatography-mass spectrometry. *Analytical chemistry* **2000**, *72*, 3653–3659.
[52] Smith DR, Robb DB, Blades MW. Comparison of dopants for charge exchange ionization of nonpolar polycyclic aromatic hydrocarbons with reversed-phase LC-APPI-MS. J Am Soc Mass Spectrom 2009;20:73–9.
[53] Yen TF, Scotti R, Espinat D, Mullins OC, Sheu EY, editors. *Structures and Dynamics of Asphaltenes*. New York, NY: Springer; 2013.
[54] Hesse M, Meier H, Zeeh B. Spektroskopische Methoden in der organischen Chemie: 102 Tabellen, 7. überarb. Aufl. Stuttgart: Thieme electronic book library; Thieme; 2005.
[55] Scherf, U.; Neher, D. *Polyfluorenes* 212; Springer Berlin Heidelberg: Berlin, Heidelberg, 2008.
[56] Abbel R, Schenning APHJ, Meijer EW. Fluorene-based materials and their supramolecular properties. J Polym Sci A Polym Chem 2009;47:4215–33.
[57] Dong B, Song D, Zheng L, Xu J, Li N. Electrosynthesis of polyfluorene in an ionic liquid and characterization of its stable electrocatalytic activity for formic acid oxidation. J Electroanal Chem 2009;633:63–70.
[58] Saari E, Perämäki P, Jalonen J. Evaluating the impact of GC operating settings on GC–FID performance for total petroleum hydrocarbon (TPH) determination. Microchem J 2010;94:73–8.